

# Arrow of time and non-Markovianity in the non equilibrium folding/unfolding of alanine decapeptide *in vacuo*

Simone Marsili, Piero Procacci

*Dipartimento di Chimica, Università di Firenze,*

*Via della Lastruccia 3, I-50019 Sesto Fiorentino, Italy and*

*Centro Interdipartimentale per lo Studio delle Dinamiche Complesse(CSDC),*

*Via Sansone 1, I-50019 Sesto Fiorentino, Italy*

(Dated: November 8, 2018)

## Abstract

We present non equilibrium molecular dynamics experiments of the unfolding and refolding of an alanine decapeptide *in vacuo* subject to a Nosé thermostat. Forward (unfolding) and reverse (refolding) work distribution are numerically calculated for various duration times of the non equilibrium experiments. Crooks theorem is accurately verified for all non equilibrium regimes and the time asymmetry of the process is measured using the recently proposed Jensen-Shannon divergence [E.H. Fend, G. Crooks *Phys. Rev. Lett*, 101, 090602] . Results on the alanine decapeptide are found similar to recent experimental data on m-RNA molecule, thus evidencing the universal character of the Jensen-Shannon divergence. The patent non markovianity of the process is rationalized by assuming that the observed forward and reverse distributions can be each described by a combination of two normal distributions satisfying the Crooks theorem, representative of two mutually exclusive linear events. Such bimodal approach reproduce with surprising accuracy the observed non Markovian work distributions.

## INTRODUCTION

Some time ago Crooks[1] derived, in the context of Monte Carlo simulations, an exact formula involving the dissipative work of a system driven out of equilibrium through a time dependent external potential and in contact with a thermal bath at temperature  $T = 1/k_B\beta$ . This formula, ever since known as the Crooks theorem (CT), reads:

$$\frac{P(x, \Lambda)}{P(\hat{x}, \hat{\Lambda})} = e^{\beta(W - \Delta F)} \quad (1)$$

where  $P(x, \Lambda), P(\hat{x}, \hat{\Lambda})$  are the probabilities of observing a forward trajectory  $x$ , giving the time schedule (or protocol)  $\Lambda$ , and of observing its conjugate trajectory  $\hat{x}$  with inverted transformation protocol  $\hat{\Lambda}$ , respectively;  $\Delta F \equiv F_B - F_A$  is the free energy difference between the initial and final canonical ensembles and  $W$  is the work done in the *forward* driven non equilibrium experiment. The Crooks formula has been later recognized of much broader validity, and it was shown to hold for deterministic systems in the context classical molecular dynamics simulations[2, 3, 4, 5], Langevin dynamics[6, 7], quantum systems[8, 9] and verified in real[10] and computer[3, 11, 12] experiments.

The essential points for Eq. 2 to hold is that the driven forward and reverse experiments ought to be started from equilibrium distributions and that the transformation protocols of the forward and reverse process (that can involve mechanical and thermodynamic variables[5] as well) are one the time reversal of the other. As the work done in the non equilibrium trajectory inverts sign by time reversal, the trajectories and their time-reversal counterpart can be labeled using the work such that Eq. 1 can thus be also written as

$$\frac{P(W|F)}{P(-W|R)} = e^{\beta(W - \Delta F)} \quad (2)$$

where  $P(W|F), P(-W|R)$  are the probability of observing a work  $W$  in the forward and reverse experiment. Eq. 2 says that trajectories that are highly dissipative (i.e.  $W - \Delta F \gg 0$ ) in the forward sense are difficult to observe in the reverse sense since for such trajectories the dissipation of its time-reversal counterpart would be negative, thus transiently violating the second law. In the functional form of Eq. 2, the Crooks theorems applies, with some provisions[13] related to the form of the external driving agent, to the controlled mechanical manipulation of a single molecule through optical tweezers[10] or atomic force microscopy.[14] We conclude this introductory remarks by stating that Eq. 2, one of the

very few *exact* equations in non equilibrium thermodynamics, holds for any regime: for instantaneous pulling we have that  $W = H_B - H_A$  and, by averaging over all trajectories, one recovers the Zwanzig[15] formula  $\langle e^{-\beta(H_B - H_A)} \rangle_A = e^{\beta\Delta F}$ . For infinitely slow pulling, i.e for quasi-static reversible transformations,  $W = \Delta F$  and the forward and backward distribution are indistinguishable and  $P(W|F) = P(-W|R) = \delta(W - \Delta F)$ .

Recently there has been considerable progress in the interpretation of non equilibrium experiments coming both from measurements on single molecules using AFM or optical traps[16] and from deterministic or stochastic simulations.[17] Feng and Crooks proposed to use the Jensen-Shannon divergence[18, 19] (JSD) between the probability of a trajectory and its time-reversal conjugate as a definition and a measure of the *time asymmetry* in a thermodynamics system. If we use the work  $W$  (which changes sign by time reversal) as a label for trajectories, then JSD can be written in terms of work distributions as

$$\begin{aligned} \text{JSD} &= \frac{1}{2} \int P(W|F) \ln \frac{2P(W|F)}{P(W|F) + P(-W|R)} dW \\ &+ \frac{1}{2} \int P(-W|R) \ln \frac{2P(-W|R)}{P(W|F) + P(-W|R)} dW. \end{aligned}$$

JSD can be shown[16] to be equal to the average gain of information about the orientation of time's arrow from one single realization of the experiment. This quantity, plotted against the average dissipation obtained in the forward and reverse driven experiments, goes to zero for reversible processes, and to one full nats of information  $\ln 2$  (i.e. 1 bit) when the two distributions do not overlap (i.e. for large average dissipation). In this latter case, it is easy to assign an observed trajectory (taken from the pool of forward and reverse non equilibrium experiments) to one of two distributions, or, stated in other words, it is easy to guess, from the analysis of one single random trajectory, in which direction the time is flowing. On such basis, when plotted against the average mean dissipation, JSD may then give indication on the energetic cost (i.e. the dissipation needed) to ensure that a molecular process (e.g. a molecular motor) advances in time. For Markovian (linear) systems, the work distributions are always Gaussian[3, 11] with variance twice the average dissipation. In this case, JSD vs dissipation is analytic and identical for all Markovian system. Therefore, Eq. 3 can also be used a measure of the non linearity of the system.

In the context of non equilibrium thermodynamics, similar concepts were put forward recently by Kawai, Parrando and Van den Broeck.[17] For system perturbed far from equilibrium through driven forward and time reversal protocols, they derived a remarkable exact

formula connecting the relative entropy of the two conjugate phase space density of system measured at the same but otherwise arbitrary point in time to the average dissipation in the forward experiment. Exploiting the fact that the system is deterministic and that the work inverts its sign by time reversal, and labeling each phase space point in terms of (future) works, the Kawai-Parrondo-Van der Broeck formula can be straightforwardly written in terms of work distribution alone as

$$\begin{aligned} \langle W \rangle - \Delta F &= k_B T D(P(W|F) || P(-W|R)) \\ &= k_B T \int dW P(W|F) \log \left( \frac{P(W|F)}{P(-W|R)} \right) \end{aligned} \quad (3)$$

Eq. 3 can be easily derived from the Crooks theorem Eq. 2. The integral on the *lhs* is the Kullback-Leibler divergence (KLD),[19] a strictly positive quantity measuring, in information theory, the expected extra message-length per datum that must be communicated if a code that is optimal for a given (wrong) distribution  $P(-W|R)$  is used, compared to using a code based on the (true) distribution  $P(W|F)$ . In general the KLD is not symmetric, i.e. if  $q, p$  are two non identical distributions,  $D(p|q) \neq D(q|p)$ . For Markovian systems, however, the KLD is always symmetric. Moreover, for such systems,  $k_B T$  times the KL divergence can be calculated analytically yielding the dissipation  $\beta\sigma^2/2$ , with  $\sigma^2$  being the variance of the Gaussian distribution. KL between forward and reverse distributions has the same characteristics of the JSD divergence, being the former like the latter both a measure of the time asymmetry (i.e. of the possibility for distinguish in which sense the time is flowing ) and of non linearity. However KL, as suggested by Kawai *et al.*, could be effectively used as a tool for obtaining a better upper bound of the free energy than the average work  $W$ . This is so since, according to the chain rule,[19] the relative entropy (or KL divergence) decreases upon coarse graining. An extremely simple coarse graining scheme could be that of approximating coarse grained histograms of the forward and backward work distribution with the best linear model satisfying the Crooks theorem. This approach has been advocated recently by Forney *et al.* [20] in the context of steered molecular dynamics of decaalanine *vacuo* along the end-to-end distance. These authors, in their so-called *FR* method[20, 21], produce a coarse grained histogram with few work measurements in both directions that are then fitted using a linear (Markovian) model. However, when the driven coordinates exhibit clear non linear effects (i.e. the noise due to all other “solvent” coordinates is not white or Gaussian), as is the case of folding and refolding of small proteins along the end-to-end

distance, then other less simplistic coarse grain schemes could and should be adopted.

In this paper we further develop the concepts of time asymmetry and coarse graining introduced in Refs. 16, 17 by presenting extensive non equilibrium molecular dynamics simulation data of unfolding and refolding process of decaalanine *in vacuo* performed with the deterministic Nosé-Hoover thermostat at 300 K. In spite of the fact that decaalanine *in vacuo* has been extensively studied in the recent past by non equilibrium computational techniques[3, 11, 20], the rationalization and interpretation of the observed data is still a matter of debate.  $\alpha$ -helix formation is also important *per se* and as a paradigm for an elementary folding/unfolding process.

Our results on decaalanine are interpreted by means of the JSD and KLD quantities above introduced. We further present a simple coarse grain and totally general model satisfying the CT based on the assumption of the occurrence, in the refolding process, of two mutually exclusive events. Such simple coarse grain dual model explains many features of the observed work distributions and can be rationalized with the existence of two competing minima for low values RC in decaalanine, i.e. one of enthalpic nature (the helix), easily accessible, in the refolding process, at low dissipation regimes, and the other of entropic origin corresponding to a manifold or misfolded coil structures which emerges at large dissipation when trying to rapidly refold decaalanine from extended structures. This view appears to be quite general and is fully consistent with the rugged funnel picture of the folding process, in the sense that escaping the rugged funnel from below is a much tamer process than reentering the funnel from above.

The present paper is organized as follows. Sec. II is dedicated to the description of the systems and of the methods used in the non equilibrium simulations. In sec. III we present the computer experiment results of the unfolding/refolding process of a single molecule of decaalanine along with a discussion focusing on the thermodynamic and microscopic aspects and on their rationalization in terms of a coarse grain description of a systems of general validity in the protein space. Conclusive remarks and futures perspective regarding the applicability of the presented methodology to real experiments are presented in Sec. IV.

## METHODS

In this section we provide the technical details on the steered molecular dynamics simulations of the Alanine deca-peptide ( $A_{10}$ ) *in vacuo*. The unperturbed system is described with the all-atom force field CHARMM whose parameters are given in Ref. 22. A constant temperature of 300 K is imposed through a Nosé-Hoover thermostat.[23] The resulting deterministic equations of motions are efficiently integrated using a reference system propagator algorithm [24] at three time steps, 3.0 fs for medium and long range non bonded interactions (no cut-off is imposed ), 1.5 fs for torsional potential involving hydrogen atoms and for short-ranged (14) non-bonded interactions, and 0.5 fs for stretching and bending potentials. The non equilibrium computer experiments from a folded ( $\alpha$ -helical) to an extended (*all trans*) structure (called *forward* process) and *viceversa* are done according to the following scheme proposed by Park and Schulten[11]. The N atom of the N-terminus residue is constrained to a fixed position and attached to the N atom of the C-terminus, though a stiff harmonic spring (i.e. by adding a stretching potential to the unperturbed Hamiltonian) of adjustable equilibrium distance of the form

$$V(t) = \frac{k}{2} [\zeta - \zeta(t)]^2 \quad (4)$$

with  $\zeta(t)$  being the time-adjustable equilibrium distance allowing the system to move along the  $\zeta$  (end-to-end distance ) coordinate. The driven unfolding (and refolding) of  $A_{10}$  along  $\zeta$  is bound to occur along the  $\alpha$ -helix axis, by means of a bending constraint imposing the N atom of the N-terminus, the N atom of the C-terminus and a distant dummy atom at fixed position to all lie on the axis of the helix. The force constant  $k$  of the external potential used for guiding the processes (Eq. 4) is 400 kcal mol<sup>-1</sup> Å<sup>-2</sup>. Such a large value is used to minimize the possible negative impact of the stiff spring approximation[11] in the calculation of the free energy between the initial and final state. The conjugated time protocols  $\Lambda$  and  $\hat{\Lambda}$  for the forward and reverse non equilibrium experiments are defined by setting in Eq. 4 the corresponding time dependent equilibrium distances  $z(t)$  and  $z(\hat{t})$  as

$$\begin{aligned} z(t) &= \zeta_i + (\zeta_f - \zeta_i) \frac{t}{\tau} = \zeta_i + v(\tau)t \\ z(\hat{t}) &= \zeta_f + (\zeta_i - \zeta_f) \frac{\hat{t}}{\tau} = \zeta_f - v(\tau)\hat{t} \end{aligned} \quad (5)$$

where  $\zeta_i$  and  $\zeta_f$  are the initial and final values of the reaction coordinate,  $\tau$  is the total (simulation) time of the non equilibrium experiment and  $v(\tau) = \pm(\zeta_f - \zeta_i)/\tau$  is the (constant)

pulling speed. In the present study, according to previous works[3, 11], we set  $\zeta_i = 15.5 \text{ \AA}$  and  $\zeta_f = 31.5 \text{ \AA}$ . The sampling at fixed value of  $\zeta$  is achieved again by using the potential of Eq. 4 with  $\zeta(t) = \zeta_i = 15.5 \text{ \AA}$  for constraining the system at the end-to-end distance of the  $\alpha$ -helix and with  $\zeta(t) = \zeta_i = 31.5 \text{ \AA}$  for constraining the system at the end-to-end distance of the all trans extended structure. In this manner, through ordinary equilibrium simulations in the canonical ensemble, we sampled, by saving the configuration at regular intervals of 2 ps, 504 initial phase-space points for the  $\alpha$ -helix state and 504 initial phase-space point for the extended state. Starting from these points, we then did forward and reverse non equilibrium molecular dynamics experiments applying the time dependent potential of Eq. 4 for various time protocols (i.e. at various pulling constant speed, corresponding to the duration  $\tau$  values of ranging from 0.021 to 4.2 ns). In particular, for *each* time protocol we did 504 forward and 504 reverse non equilibrium experiments for a total simulation time of 11.15  $\mu s$ . All non equilibrium simulations were done in parallel on a 32 node Intel CPU X9650 cluster using an in-house parallel version of the program orac[25]. The work done on  $A_{10}$  in each of the non equilibrium experiments is calculated through

$$W = \int_0^\tau K(\zeta - \zeta(t))v(\tau)dt \quad (6)$$

## RESULTS AND DISCUSSION

In Fig 1 we show the forward (unfolding)  $P(W|F)$  and backward (refolding) ( $P(-W|R)$ ) work distribution obtained with the various time protocols by means of the computational methods described in the previous section. As expected, the two conjugated work distributions approach to each other the longer the duration of the non equilibrium experiment, i.e. the more reversibly is done the transformation. The conjugated work distributions appear to meet approximately at the same value of  $W = \Delta F$  no matter what time protocol is used, in full agreement with the Crooks theorem 2. The free energy difference  $\Delta F$  between the helix ( $\zeta = 15.5 \text{ \AA}$ ) and the extended ( $\zeta = 31.5 \text{ \AA}$ ) structure can be estimated with rather good accuracy using the Bennett acceptance ratio[26, 27] formula already starting from  $\tau = 0.105 \text{ ns}$ , where the two work distribution overlap significantly. Using the Bennett formula, we consistently obtain values between 92 and 94 kJ/mol, with an average value of  $\Delta F = 93.3 \pm 0.5 \text{ kJ/mol}^{-1}$  in full agreement with previous estimate of the unfolding free energy of decaalanine[3, 11]. Detailed data regarding  $\Delta F$ , dissipated work and variance of

the distributions are reported in Table I. From Inspection of a Figure 1 and from the data of Table I we see that, while the forward distribution  $P(W|F)$  preserves an approximately Gaussian shape for all time protocols, the reverse distribution show a markedly non Gaussian shape at all times. In particular, the reverse distributions are characterized by a long tail that, for  $\tau < 0.1$  ns and  $\tau > 0.2$  ns, lies on the right and of the left of the maximum of the distribution, respectively. As we shall see later in the discussion, this peculiar behaviour of the non equilibrium refolding of  $A_{10}$  is a signature of competitive mutually exclusive events, i.e. the formation of the  $\alpha$ -helix (for  $W > 60$  kJ mol<sup>-1</sup>, i.e. at low dissipation) form one hand and the evolution towards *misfolded* structures (for  $W < 25$  kJ mol<sup>-1</sup>, i.e. at high dissipation) form the other hand.

The asymmetry in the behaviour of  $P(W|F)$  and  $P(W|R)$  distribution in  $A_{10}$  is shown in Fig. 2 where we report the forward and reverse dissipation (see also Table I) against the duration time  $\tau$  of the non equilibrium forward and reverse experiments. The reverse process is consistently more dissipative than the forward for all duration time. Beyond 1 ns, the dissipation for the reverse and forward processes becomes identical and small compared to  $\Delta F$ , indicating that the non equilibrium experiments are performed in conditions of *quasi*-reversibility. Such behaviour of the dissipation of the refolding process *vs* the duration time of the non equilibrium experiment could have been easily guessed directly form Fig. 1 by following the trends of the maxima of the distributions as function of the duration time of the experiments. The “transition time” between reversible and *quasi*-reversible regimes (approximately falling between 0.8 and 1.5 ns) must be ultimately connected to either the non equilibrium time protocol or to some inherent structural property (e.g. potential of mean force along  $\zeta$ ) and dynamical property (e.g. friction and diffusion coefficients along  $\zeta$ ) of the system under investigation or, again, to both.

In order to assess the time-asymmetry and non linearity of  $A_{10}$ , the data are used to compute the Jensen-Shannon divergence as a function of the average dissipation  $\mathcal{D} = \frac{1}{2}(\langle W \rangle_f + \langle W \rangle_r)$  in  $k_B T$  units. To this aim we use directly Eq. 3 which can be applied to the work data without any a priori knowledge of  $\Delta F$ . The results (triangle symbol) are reported in Fig. 3. The solid line correspond to the universal Markov model where  $P(W|F)$  and  $P(-W|R)$  are normal distributions with equal variance and with variance and dissipation related by  $\langle W \rangle - \Delta F = \beta \frac{\sigma^2}{2}$ . Expectedly, the JSD follows closely the Markov model for average dissipation below  $4 k_B T$ , i.e. when the process is quasi-reversible and above  $13 k_B T$



i.e. when the two distributions have negligible overlap and the time asymmetry approaches its limiting values of  $\ln 2$  nats. Remarkably, this limiting value of the JSD is reached at an average dissipation that is close to the corresponding dissipation that can be extrapolated from the experimental data on the unfolding/refolding of RNA molecule reported recently by Feng and Crooks (see Fig. 2 of Ref. 16). This suggests a universal behaviour of the JSD in real systems, thereby strengthening the idea [16] that the encoding cost to ensure that a molecular process advances in time amounts to few  $k_B T$ , being rather insensitive to specificity of the molecular process itself.

In spite of the non linearity (see Table I and Fig. 2) of  $A_{10}$  along  $\zeta$ , especially evident at intermediate dissipation regimes (i.e for  $0.1 < \tau < 0.5$  ns), the Jensen-Shannon divergence *vs* dissipation appears quite insensitive to such non linearity being nearly indistinguishable from the universal Markov Jensen-Shannon divergence (solid line) for all dissipation energies. We must stress here that the error in the Jensen-Shannon divergence *vs* dissipation is small (with error bars of the order of the height of the triangle symbols in Fig. 3), reflecting the small error in the determination of  $\Delta F$  itself. In order to show this more quantitatively, we have also calculated the JSD using the alternative Eq. 7 of Ref. 16 which requires a prior knowledge of  $\Delta F$  (through, e.g., the Bennett’s method). As one can see from Fig. 3, the JSD calculated with this method (circle symbol) follows closely that of the direct method Eq. 3. The insensitivity of JSD *vs* the mean dissipation to the non linearity of the system is probably due to the fact that the JSD itself is a symmetries average of the two Kullback divergence between the forward and reverse distribution with respect to the *average* of the two distributions.

The non linearity of the folding/unfolding process of  $A_{10}$  for  $\tau < 1$  ns does not allow the use of a simple Markov approach to satisfactorily reproduce, in this time range, the observed distribution and at the same time satisfy the CT. As an example of such inability, in Fig. 4 we show the best Markov model fitting the data for  $\tau = 0.105$ ,  $\tau = 0.21$  ns and at the same time satisfying the Crooks theorem with  $\Delta F = 93.3$  KJ mol<sup>-1</sup>. The inadequacy of the Markov model is not surprising since the driven end-to-end distance is not a “good” coordinate, i.e. the modulations of remaining (“solvent”) coordinates on  $\zeta$  do not produce a white noise. The memory effects in  $\zeta$  (see e.g Fig 2) indicate that there must be some other important orthogonal coordinate besides  $\zeta$  that should be included in the model. We stress here that the pure Markov model is a coarse graining of the information regarding

the microscopic detail of process in the sense that one attempts to describes the the full information given by the experimental histograms of the forward and reverse work with two CT related Gaussian. This elementary coarse-graining is the so-called *FR* model[21].

In an effort to go beyond the simple Markov model or *FR* model, following Feng and Crooks[16], we now assume that the forward and reverse true distributions  $P(W|F)$ ,  $P(-W|R)$  can be approximated by the distributions  $\mathcal{P}(W|F)$ ,  $\mathcal{P}(-W|R)$ , each given by a linear combination of *two* normal distributions. i.e.

$$\begin{aligned}\mathcal{P}(W|F) &= p\mathcal{N}(w_1, \sigma_1) + (1 - p)\mathcal{N}(w_2, \sigma_2) \\ \mathcal{P}(-W|R) &= q\mathcal{N}(w_1 - \beta\sigma_1^2, \sigma_1) + (1 - q)\mathcal{N}(w_2 - \beta\sigma_2^2, \sigma_2)\end{aligned}\quad (7)$$

where  $\mathcal{N}(w, \sigma)$  is a normal distribution with mean  $w$  and variance  $\sigma$  and  $0 \leq p \leq 1$ . The form of  $\mathcal{P}(-W|R)$  is a trivial consequence of the CT, Eq. 2. Eq. 7 implies that the forward non equilibrium process is described by two mutually exclusive events occurring with probability  $p$  and  $(1 - p)$  in the forward process and  $q$  and  $1 - q$  in the reverse process with mean dissipation satisfying the Crooks theorem. We stress here that also such bimodal scheme is a coarse graining of the full available microscopic information provided by the experimental histogram  $P(W)$ 's. The model can be of course complicated by combining an arbitrary number of normal distributions allowing for many competing events. However, we shall see in the forthcoming discussion that the simple bimodal scheme, Eq. 7, captures the essential features of the “experimental” distributions based on the full microscopic information.

Going back to Eq. 7, the probabilities  $p$  and  $q$  are not free parameters as the the CT and the normalization condition set a twofold constraint on the coefficients of the combinations. In fact, by using the Crook theorem, Eq. 2, in Eq. 7, the condition of normalization on the probability densities  $P(W|F)$  and  $P(-W|R)$  requires that

$$\begin{aligned}p &= \frac{1 - e^{\beta(\Delta F - w_2 + \frac{1}{2}\beta\sigma_2^2)}}{e^{\beta(\Delta F - w_1 + \frac{1}{2}\beta\sigma_1^2)} - e^{\beta(\Delta F - w_2 + \frac{1}{2}\beta\sigma_2^2)}} \\ q &= \frac{(1 - e^{\beta(\Delta F - w_2 + \frac{1}{2}\beta\sigma_2^2)})e^{\beta(\Delta F - w_1 + \frac{1}{2}\beta\sigma_1^2)}}{e^{\beta(\Delta F - w_1 + \frac{1}{2}\beta\sigma_1^2)} - e^{\beta(\Delta F - w_2 + \frac{1}{2}\beta\sigma_2^2)}}\end{aligned}\quad (8)$$

Since  $p$  and  $q$  are probabilities, not all the values of the free parameters  $w_1, \sigma_1, w_2, \sigma_2$  are allowed. We now define the variables  $x = \Delta F - w_1 + \frac{1}{2}\beta\sigma_1^2$  and  $y = \Delta F - w_2 + \frac{1}{2}\beta\sigma_2^2$ . In Fig. 5 we plot the functions  $p(x, y)$  and  $q(x, y)$  on the domain of the variables  $x = \Delta F - w_1 + \frac{1}{2}\beta\sigma_1^2$  and  $y = \Delta F - w_2 + \frac{1}{2}\beta\sigma_2^2$ , for which  $0 \leq p \leq 1$  and  $0 \leq q \leq 1$ . As it is well known, the

allowed values for the variance and the mean in a pure Markov model obeying the Crooks theorem stays on the line  $w = \Delta F + \beta\sigma^2/2$ . Analogously, Figure 5 represents the two dimensional domain set by the CT theorem for a bimodal Markov model. When  $p = 1$ , then  $e^{\beta(\Delta F - w_1 + \frac{1}{2}\beta\sigma_1^2)} = 1$  such that  $\Delta F - w_1 = \frac{1}{2}\beta\sigma_1^2$  and  $q = 1$ , thus recovering the single Gaussian Markov model.

We now adopt the model based on the coarse grain bimodal representation Eq. 7, in order to reproduce the true work distributions. In Table II we report the parameters obtained from the fit using the bimodal distributions as a function of the duration time. The loss of information due to coarse graining with respect to the true (measured) distribution is measured by the KL divergence (Eq. 3) between the mean of the true distributions  $P(W|F) + P(-W|R)$  and the mean of the (absolutely continuous) coarse grain distribution  $\mathcal{P}(W|F) + \mathcal{P}(-W|R)$ . Large values of KL means great loss of information in the coarse graining.

We see that the bimodal approach, Eq. 7 has consistently smaller KL's with respect to the purely Markov model (shown in III) at all times. A visual example of the surprising accuracy of Eq. 7 in reproducing the true distributions is shown in Fig. 5 where the true distributions and the bimodal distribution of Eq. 7 are compared for various short and intermediate duration times. By inspection of Table III, one can see that the relative probability of the two mutually exclusive event underlying the reverse distribution depends on the rate with which the non equilibrium experiment is done. At short duration times ( $\tau = 0.021$  ns), the highly dissipative events in the refolding of Alanine decapeptide are overwhelmingly more likely than the non dissipative event, while *most* of the “refolding” trajectories produce a misfolded structure with  $\zeta = 15.5$  Å. When the rate of the non equilibrium experiment is slower (e.g. at  $\tau = 0.21$  or  $\tau = 0.3$  ns), then the two competing event (misfolding *vs* folding) becomes of comparable probability. Expectedly, in the unfolding process for all duration duration times, the dissipative event has consistently a much larger probability than the non dissipative event (see Table III). In fact, while on one hand the misfolding of  $A_{10}$  starting from an extended structure is a probable outcome in a fast refolding process, on the other hand in the non equilibrium unfolding process it is not so likely to disrupt the helix doing *less* work than the needed reversible work. Remarkably, the CT automatically balances these mutually dependent probabilities  $p$  and  $q$  through Eq. 9.

The results that we have presented show that a coarse grain scheme based on only two mutually exclusive linear event, yielding a work distribution that is a combination of two

Gaussian distributions with linear coefficients satisfying the Crooks theorem, explains the observed non linear work distributions at short and intermediate times with surprisingly good accuracy. The success of the bimodal approach in reproducing the essential features of the true distributions at short and intermediate duration times of the non equilibrium experiments allows to sketch out an elementary microscopic picture: in the forward direction only one path is possible and the process is approximately Markovian. In the reverse direction (refolding), several other metastable minima at  $\zeta = 15.5 \text{ \AA}$  can be visited depending on the dissipation (i.e. on the duration time of the experiment). At very fast rate, virtually no hydrogen bond has to time to form and a misfolded coil structure is systematically formed. At intermediate rates more paths are possible towards variously misfolded structure (included distorted helices) with a probability balance between these paths that depends on the the duration time (i.e on the mean dissipation): the slower the process, the smaller the dissipation, the larger is the fraction of refolding trajectories producing the helix. At duration time between 0.6-2 ns, the refolding process ends up *mostly* in the helical structure. For duration time beyond 3 ns, refolding is virtually non dissipative (reversible) and only the  $\alpha$ -helix minimum is visited. The existence of the misfolded minima at  $\zeta = 15.5 \text{ \AA}$ , that have a negligible probability at the canonical equilibrium, emerges in the refolding process in the fast pulling/large dissipation regime. The rare event in these dissipative regimes is the correct folding of decaalanine to the enthalpic minimum. As the regime becomes less and less dissipative (i.e more reversible), the rare event becomes the formation of misfolded coils. The dissipation in the refolding process, that can be simply modulated by varying the duration time of the non equilibrium experiment, may be thus a mean to “see” minima in the folded (or native) structure that are hard to detect at equilibrium.

## CONCLUSION

In this paper we have studied the Alanine decapeptide in vacuo at 300 K and analyzed its behaviour in driven out of equilibrium classical molecular dynamics simulations. Applying an external potential, we produced classical trajectories starting form the  $\alpha$ -helix structure and ending to a fully extended *all trans* structure and *viceversa*. The bidirectional non equilibrium experiments were done at various pulling rate, with duration time ranging from 0.021 ps to 4.2 ns. For each bidirectional experiment at a given pulling rate we calculate the

forward and reverse work distribution and apply the Bennett acceptance ratio to estimate the free energy difference between the folded and unfolded state, thus evaluating the dissipative work spent during the non equilibrium processes. We found that the folding/refolding process is markedly non Markovian for duration time  $t < 1$  1-1.5 ns and that in such pulling rate regime the reverse process consistently dissipates more than the forward counterpart. For duration time  $\tau > 2$  ns, the system becomes reversible, exhibiting equal forward and reverse mean dissipation  $W_d = \beta\sigma^2/2$  with the  $\sigma^2$  being the variance of two identical normal distributions. Using our non equilibrium trajectories of  $A_{10}$  and the corresponding work distributions, we have measured the Jensen-Shannon divergence as a function of the mean forward and reverse dissipation. This quantity is a convenient metric for the “irreversibility” of the system, i.e. for the ability, given a pulling regime yielding a given mean dissipation, to figure out in which direction time is flowing from one random realization of the experiment. Remarkably, the behaviour of the Jensen-Shannon divergence for the Alanine decapeptide *in vacuo* closely follows that observed in a recent single RNA molecule experiment,[10] thereby strengthening the recently proposed idea [16] that the encoding cost to ensure that a molecular process advances in time is independent of the system and amounts to 4-10  $k_bT$ . In the case of the Alanine decapeptide, which shows a strongly non linear behaviour, the Jensen-Shannon divergence plotted against the dissipation has been nonetheless found to approximately follow the JSD for a purely Markov model. Such surprising insensitivity of the JDS *vs* dissipation to non linearity is yet another confirmation of its universal character.

The observed forward and reverse work distributions in  $A_{10}$  cannot be fitted satisfactorily for fast and intermediate pulling speed with normal distributions satisfying the Crooks theorem, thereby reflecting the fact that the process in such regimes is non Markovian (i.e. the end-to-end coordinate exhibits memory effects). Alanine decapeptide behaves linearly only for sufficiently slow pulling rates ( $\tau \geq 1$  ns ). Following a suggestion by Feng and Crooks[16], we thus fitted the observed distribution using combination of two normal distributions. This approach implies that both the forward and the reverse process can be described by two rather than one solvent modulated processes, whose relative probability (i.e. the ratio of the linear coefficients of the combination) is regulated by the Crooks theorem and by the pulling rate of the non equilibrium experiment. We found that such a simple model can reproduce with surprising accuracy the observed distributions at short and intermediate pulling rate. At short rates the reverse distribution has an overwhelmingly large component

from the normal distribution with mean corresponding to large dissipation, with a negligible contribution arising from a rare non dissipative event corresponding to the refolding in the  $\alpha$ -helix structure. For short and intermediate duration times, the “refolding” of  $A_{10}$  has an high chance to fail producing a manifold of misfolded structures. As the duration time grows, the likelihood of the non dissipative process (i.e. the correct refolding) grows as well. The break-even point for the likelihood of two events in the reverse driven process occurs between duration times of 0.2 and 0.3 ns. The above results suggests a possible route in real experiments on single molecules using, e.g., an optical trap apparatus to detect metastable states. In fast pulling experiments, the extra energy implied in the large dissipation allows to visit states that are hard to visit in a driven quasi reversible experiment. In presence of two competing minima, one could then use the dual Markov model extrapolated from few bidirectional work measurements to both achieve, trough the KL divergence, and its connection to the dissipation, a better estimate of the free energy between the final and initial states and to identify secondary metastable minima at fixed driven coordinate that are difficult to evaluate either because of the presence of high barrier or because they are several  $KT$  larger than the principal (native) structure.

- 
- [1] G. E. Crooks, J. Stat. Phys. **90**, 1481 (1998).
- [2] D. J. Evans, Mol. Phys. **101**, 1551 (2003).
- [3] P. Procacci, S. Marsili, A. Barducci, G. F. Signorini, and R. Chelli, J. Chem. Phys. **125**, 164101 (2006).
- [4] E. Schöll-Paschinger and C. Dellago, J. Chem. Phys. **125**, 054105 (2006).
- [5] R. Chelli, S. Marsili, A. Barducci, and P. Procacci, Phys. Rev. E **75**, 050101 (2007).
- [6] J. Kurchan, J. Phys. A: Math Gen. **31**, 3719 (199).
- [7] T. Ohkuma and T. Ohta, J. Stat. Mech-Theory E. p. P10010 (2007).
- [8] Tasaki H, Jarzynski relations for quantum systems and some applications, 2000 arXiv:cond-mat/0009244.
- [9] P. Talkner, M. Campise, and P. Hanggi, J. Stat. Mech. p. P020205 (2009).
- [10] D. Collin, F. Ritort, C. Jarzynski, S. B. Smith, I. Tinoco, and C. Bustamante, Nature **437**, 231 (2005).
- [11] S. Park and K. Schulten, J. Chem. Phys. **120**, 5946 (2004).
- [12] R. Chelli, S. Marsili, A. Barducci, and P. Procacci, J. Chem. Phys. **127**, 034110 (2007).
- [13] G. Hummer, J. Chem. Phys. **114**, 7330 (2001).
- [14] A. Imparato, F. Sbrana, and M. Vassalli, Eur. Phys. Letters **82**, 58006 (2008).
- [15] R. W. Zwanzig, J. Chem. Phys. **22**, 1420 (1954).
- [16] E. H. Feng and G. Crooks, Phys. Rev. Lett. **101**, 090602 (2008).
- [17] R. Kawai, J. M. R. Parrondo, and C. V. der Broeck, Phys. Rev. Lett. **98**, 080602 (2007).
- [18] J. Lin, IEEE Trans. Inf. Theory **37**, 145 (1991).
- [19] T. Cover and J. A. Thomas, eds., *Elements of information theory* (Wiley, New Jersey, 2006).
- [20] M. W. Forney, L. Lanosi, and I. Kosztin, Phys. Rev. E **78**, 051913 (2008).
- [21] I. Kosztin, B. Barz, and L. Janosi, J. Chem. Phys. **124**, 064106 (2006).
- [22] A. Mackerell, D. Bashford, M. Bellot, R. Dunbrack, J. Evanseck, M. Field, J. Gao, H. guo, S. Ha, D. Joseph-Mcarthy, et al., J. Phys. Chem. B **102**, 3586 (1998).
- [23] S. Nosé, Mol. Phys. **52**, 255 (1984).
- [24] M. Marchi and P. Procacci, J. Chem. Phys. **109**, 5194 (1998).
- [25] P. Procacci, T. A. Darden, E. Paci, and M. Marchi, J. Comp. Chem. **18**, 1848 (1997).

- [26] M. R. Shirts, E. Bair, G. Hooker, and V. S. Pande, *Phys. Rev. Lett.* **91**, 140601 (2003).
- [27] C. H. Bennett, *J. Comput. Phys.* **22**, 245 (1976).



## Tables

$\tau$	$\Delta F$	$\langle W_f^d \rangle$	$\sigma_f^2$	$\langle W_r^d \rangle$	$\sigma_r^2$
0.021	86.0	83.2	245.6	82.8	67.7
0.042	84.2	60.4	174.6	72.9	142.0
0.063	94.0	40.6	133.4	75.2	282.4
0.084	92.3	34.7	114.0	65.3	406.2
0.105	93.8	28.6	105.8	59.5	489.5
0.150	93.9	22.8	75.6	46.6	507.8
0.210	93.7	18.6	69.4	35.6	434.0
0.300	93.9	14.1	54.4	25.6	303.9
0.420	92.9	12.0	52.1	18.3	204.4
0.630	93.0	8.7	42.8	11.9	105.9
0.840	93.2	7.1	32.6	9.2	79.4
0.930	93.6	6.3	30.1	8.4	88.3
1.050	93.2	5.8	24.8	7.9	85.5
2.100	93.4	3.2	16.3	3.9	40.4
4.200	93.2	1.7	9.7	2.3	33.4

TABLE I: Salient data of the work distributions in Alanine deca-peptide *in vacuo* at 300 K. For each duration time  $\tau$ , the forward and reverse work distributions have been calculated using 504 trajectories.  $\Delta F$  is the free energy difference between the final (all trans extended structure,  $\zeta = 31.5 \text{ \AA}$ ) and the initial ( $\alpha$ -helix structure,  $\zeta = 15.5 \text{ \AA}$ ) using the Bennett acceptance ratio[26] on the 1008 forward and reverse trajectories.  $\langle W_f^d \rangle$ ,  $\sigma_f^2$ ,  $\langle W_r^d \rangle$ ,  $\sigma_r^2$  are the mean dissipated work and variance of the forward and reverse work distributions, respectively

$\tau$	KL	Forward distribution					Reverse distribution				
		$p$	$w_1$	$\sigma_1$	$w_2$	$\sigma_2$	$q$	$w_3$	$\sigma_3$	$w_4$	$\sigma_4$
0.021	0.38	1.00	167.38	314.83	21.44	47.49	0.99	2.40	47.49	41.15	314.83
0.042	0.55	1.00	143.35	222.69	31.04	60.63	0.90	6.73	60.63	54.06	222.69
0.063	0.48	1.00	134.87	187.48	41.19	72.37	0.82	12.17	72.37	59.69	187.48
0.084	0.60	1.00	126.43	144.10	99.73	199.01	0.84	19.94	199.01	68.65	144.10
0.105	0.43	1.00	122.30	126.78	118.34	231.15	0.79	25.65	231.15	71.47	126.78
0.150	0.51	0.99	115.49	97.68	131.40	240.41	0.69	35.00	240.41	76.32	97.68
0.210	0.42	0.98	111.76	82.83	124.30	199.57	0.59	44.28	199.57	78.55	82.83
0.300	0.33	0.97	107.78	65.06	115.62	149.68	0.51	55.60	149.68	81.69	65.06
0.420	0.41	0.97	104.62	52.95	113.55	133.20	0.65	83.39	52.95	60.14	133.20
0.630	0.31	0.99	102.49	44.96	106.00	97.50	0.82	84.46	44.96	66.91	97.50
0.840	0.37	1.00	102.07	44.96	113.08	148.18	0.98	84.04	44.96	53.67	148.18
0.930	0.27	1.00	100.17	35.42	99.68	123.54	0.97	85.97	35.42	50.15	123.54
1.050	0.31	1.00	99.40	31.53	102.81	124.17	0.97	86.76	31.53	53.02	124.17
2.100	0.27	0.99	96.26	16.09	115.83	123.66	0.98	89.81	16.09	66.25	123.66
4.200	0.14	0.89	94.56	7.41	96.67	21.06	0.86	91.59	7.41	88.23	21.06

TABLE II: Best fit parameters for the true forward and reverse distributions, using a bimodal distribution Eq. 7.  $\tau$  is the duration time of the non equilibrium experiment in ns.  $KL$  is the Kullback-Leibler divergence (in kJ units) between the sum of the true forward and reverse distribution and the sum of the fitted bimodal forward and reverse distributions.  $w_3 \equiv w_1 - \beta\sigma_1^2$  and  $w_4 \equiv w_2 - \beta\sigma_2^2$  are the mean value of the normal distribution of the reverse process. For the meaning of the other symbol see text. Units of energy are  $\text{kJ mol}^{-1}$ .

$\tau$	KL	$w$	$\sigma$
0.021	2.20	177.6	421.811
0.042	5.14	176.6	416.912
0.063	6.16	172.2	395.072
0.084	7.25	130.5	187.082
0.105	7.06	125.9	164.197
0.150	7.98	117.7	123.593
0.210	5.13	114.1	105.130
0.300	3.23	109.5	81.816
0.420	3.01	105.6	62.393
0.630	1.44	102.2	45.533
0.840	1.01	100.3	36.747
0.930	1.95	98.9	29.519
1.050	1.80	99.4	31.581
2.100	1.92	96.1	15.379
4.200	0.32	94.7	8.348

TABLE III: Best fit parameters of the true forward and reverse distribution using the linear model.  $KL(\text{kJ mol}^{-1})$  is the Kullback-Leibler divergence between the sum of the true forward and reverse distributions and sum of the fitted Gaussian forward and reverse distributions.

## Figure Captions

- Fig. 1** Forward (on the right in brown) and backward (on the left in black) work distributions for Alanine decapeptide *in vacuo* at 300 K obtained in non equilibrium experiments of various duration time ranging, from bottom to top, from 0.021 s to 4.2 ns. Each forward and reverse distribution has been calculated using 504 work measurements.
- Fig. 2** Mean dissipation *vs* the duration time of the non equilibrium experiments for the forward (unfolding) and reverse (refolding) of Alanine decapeptide *vacuo*.
- Fig. 3** Jensen-Shannon divergence *vs* the mean dissipation  $0.5(\langle W_f \rangle + \langle W_r \rangle)$  in Alanine decapeptide *vacuo* at 300 K. The triangle symbols have been calculated according to Eq. 3. The circle have calculated using Eq. 7 of Ref. 16 by using a  $\Delta F$  of  $93.3 \text{ kJ mol}^{-1}$ . The solid line refers to a Gaussian (Markovian) model such that  $\langle W_d \rangle = \beta\sigma^2/2$  in both forward and reverse directions.
- Fig. 4** (a): Forward (circle and solid line) and reverse (triangle and dotted line) distribution for a duration time of  $\tau = 0.105 \text{ ns}$  in  $A_{10}$  *in vacuo* at 300 K compared with the best fit Markov model (solid and dashed thick lines ) satisfying Eq. 2.  
 (b): Same as in a) except for a duration time of  $\tau = 0.210 \text{ ns}$ .
- Fig. 5** Probabilities  $p$  and  $q$  (see Eq. 9) for a bimodal distribution satisfying the CT (Eq. 2) as a function of  $x = \Delta F - w_1 + \frac{1}{2}\beta\sigma_1^2$  and  $y = \Delta F - w_2 + \frac{1}{2}\beta\sigma_2^2$  ( $RT$  units).
- Fig. 6** True and fitted forward and reverse work distributions in Alanine decapeptide *in vacuo* at 300 K for various duration times of the non equilibrium experiments using the bimodal approach, Eq. 7. The forward and reverse true distribution are in brown and black, respectively. The forward and reverse fitted distribution are in violet and blue, respectively. The parameters of the fit can be found in Table II.

FIG. 1:

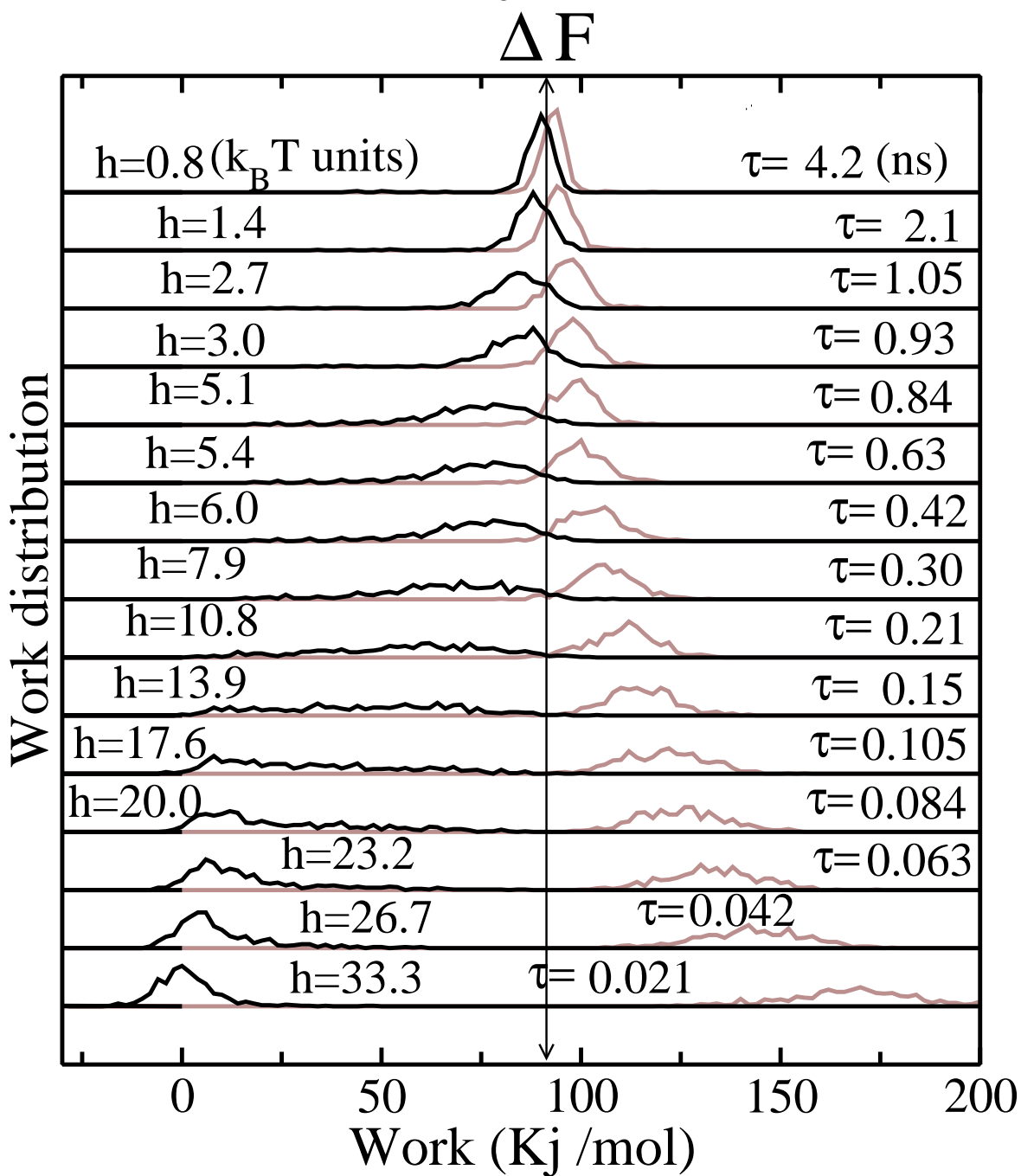


FIG. 2:

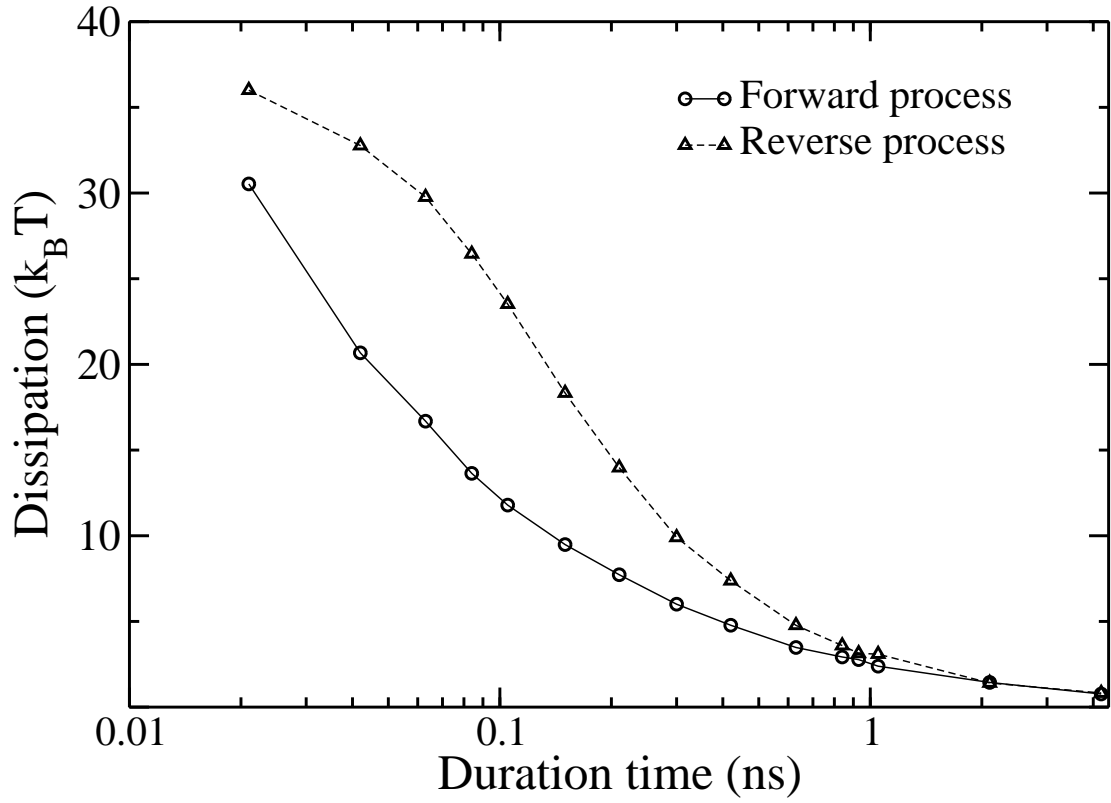


FIG. 3:

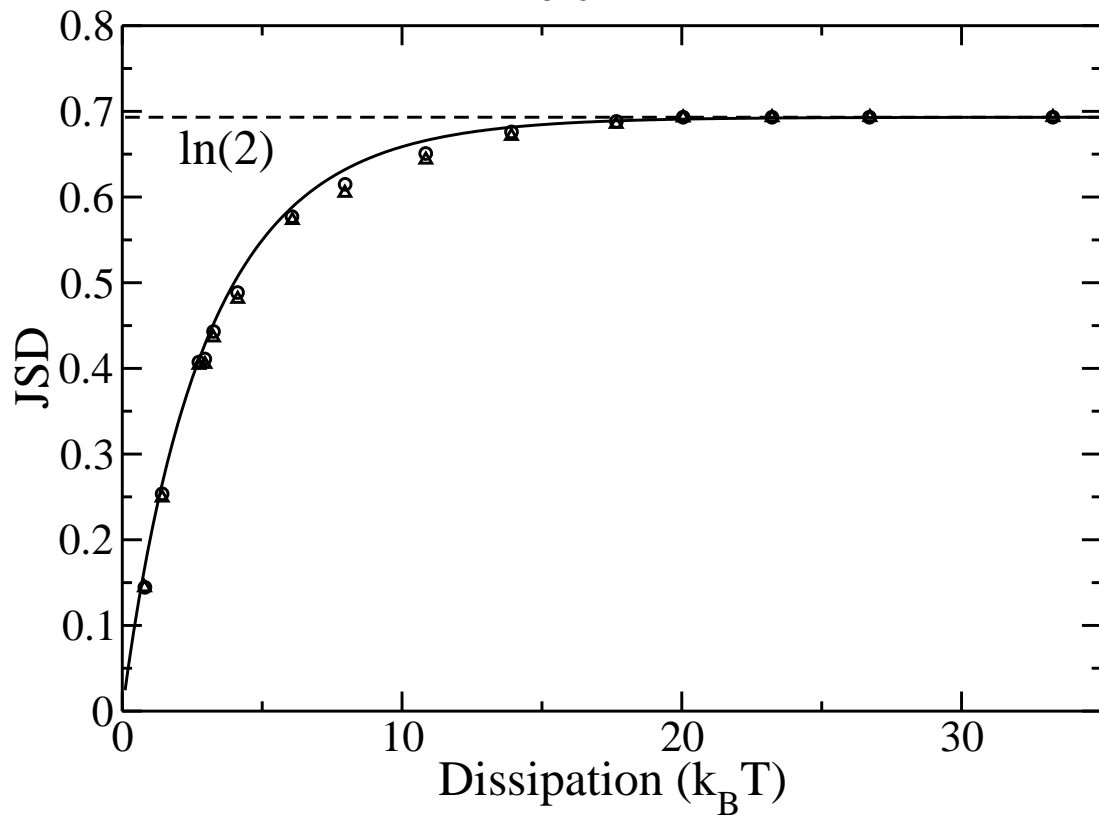


FIG. 4:

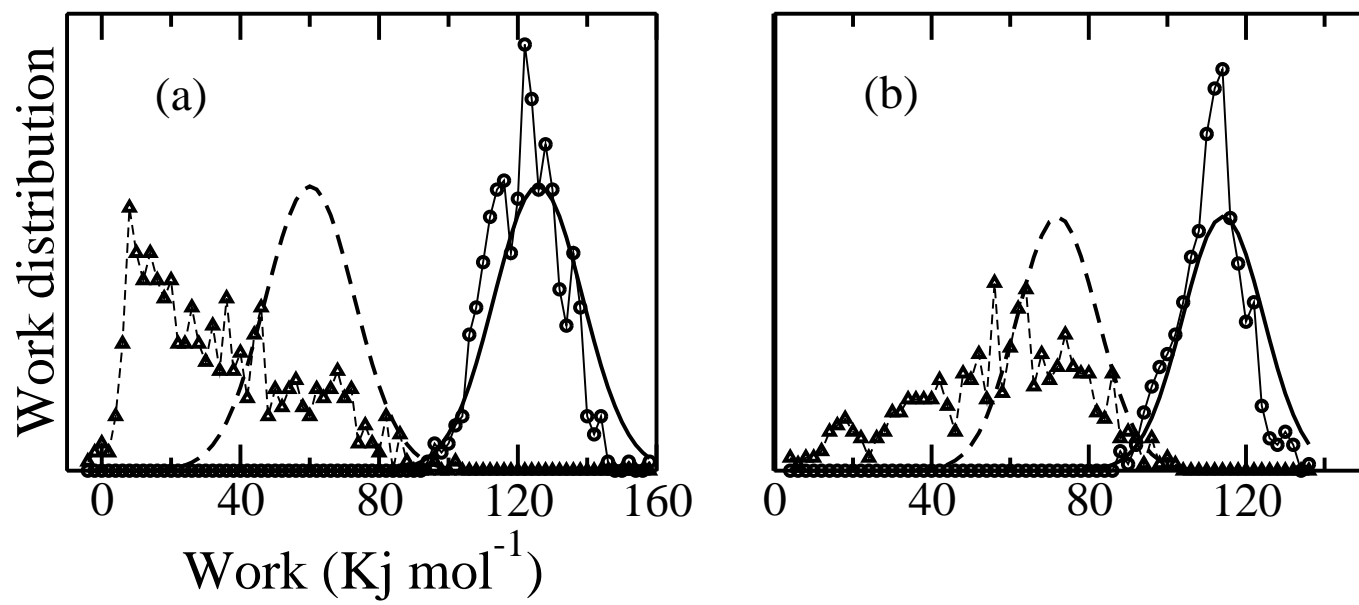




FIG. 5:

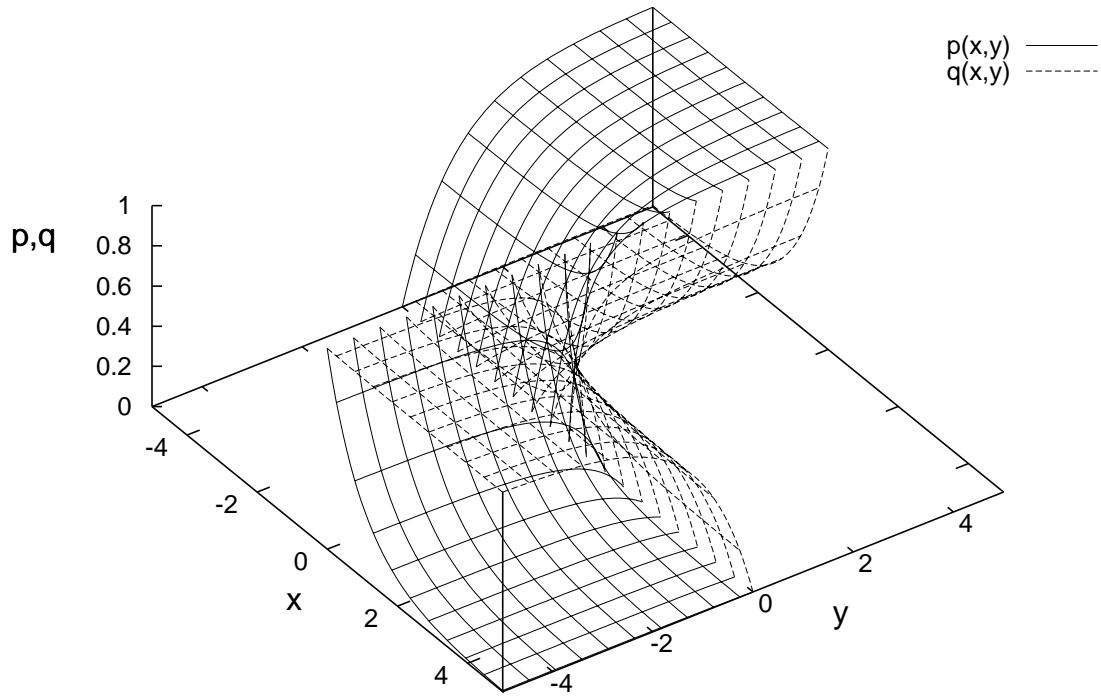


FIG. 6:

